Distillation of Squeezing using an engineered PDC source

Thomas Dirmeier,[1,2] Johannes Tiedau,[3] Imran Khan,[1,2] Vahid Ansari,[3] Christian R. Müller,[1,2] Christine Silberhorn,[3] Christoph Marquardt,[1,2] and Gerd Leuchs[1,2]

[1] *Max Planck Institute for the Science of Light, Staudtstr. 2, 91058 Erlangen, Germany*
[2] *Friedrich-Alexander-Universität Erlangen-Nürnberg (FAU),*
Department of Physics, Staudtstr. 7/B2, 91058 Erlangen, Germany
[3] *Integrated Quantum Optics, Paderborn University,*
Warburger Str. 100, 33098 Paderborn, Germany
(Dated: July 19, 2019)

We demonstrate homodyne detection of quantum states originating from a genuinely spatially and temporally singlemode parametric downconversion source in non-linear waveguides. By using single photon subtraction, we implement the distillation of squeezed states witnessing an improvement of 0.1 dB from an intial squeezing value of 1.62 ± 0.01 dB, while achieving a purity of 0.58, and confirm the non-Gaussianity of the distilled state via the higher order cumulants. With this we demonstrate the sources suitability for scalable hybrid quantum network applications.

The quantized nature of light fields manifests itself by the discretization of their energy content. But this property does not provide any information about the underlying spatio-temporal mode structure. While monochromatic fields defined as standing waves in a box are typically taken as the standard formalism for field quantization, practical systems seldomly fulfill such clean theoretical conditions. The precise experimental control of the spatial and temporal degrees of freedom of quantum light has remained one of the major challenges of quantum state engineering in the last decade.

Parametric downconversion (PDC) processes have become the prevalent source for quantum light generation due to their simplicity in implementation and their flexibility for state control. The spatial modes of the prepared states can readily be specified by either introducing a cavity geometry [1–3] or by using waveguiding structure in a non-linear medium [4–6] and is in most experiments designed to be singlemode. On the contrary, the temporal mode structure of the generated state is highly multimode and narrow-band filtering is frequently applied. This however is not suitable for pulsed light which is composed of many frequencies forming a coherent wavepacket. In this scenario, we can define field orthogonal pulsed temporal modes (TM) which in recently have been identified as a resource for multi-dimensional quantum networking and techniques to control those parameters are under development [7, 8]. In particular, these techniques have allowed us to limit the TM content up to a single mode which is one of the key achievements in the efficient generation of pure heralded single photons [4, 5, 9–12]. This ability is a prerequisite for pulsed quantum networking applications which rely on the synchronization of state conditioning to realize scalable measurement-based quantum information schemes with probabilistic outcomes.

In such applications, one generally distinguishes between continuous and discrete variable protocols which effectively only depend on the way the light is detected in the final processing step. The single photon generation is understood in the context of discrete variable (DV) systems where the photon counting methods are insensitive to TMs which motivated the state engineering efforts. Still, current linear network applications suffer significantly from the trade-off between having noise contributions from multiphoton components and detection rates [13]. In the framework of continuous variables (CV), multiphoton contributions in PDC are directly translated into a higher degree of squeezing. Additionally, homodyne detection provides an effective filtering on TMs determined by the local oscillator (LO), however the detection method restricts the toolbox of quantum information operations to Gaussian ones. This has been shown to be insufficient for many pivotal quantum information protocols, such as entanglement distillation [14] or quantum computation with quantum advantage [15, 16]. One way to overcome this limitation is by combining both frameworks in hybrid information processing schemes [17]. The realization of CV entanglement distillation has been the prominent example of hybrid systems [18–29], but these experiments have also revealed the difficulties when dealing with TM multimode sources and a priori incompatible CV/DV detection apparati most of which can be attributed to the need of optical filtering which is necessary due to challenging mode-matching requirements.

In this letter, we perform homodyne detection on an engineered PDC source of pulsed squeezed states with spatial and temporal singlemode characteristics and demonstrate squeezing distillation via photon subtraction with high efficiency and state purities. This highlights the suitability of our single-pass source based on an engineered non-linear waveguide to realize hybrid quantum information processing protocols in scalable optical setups.

Considering a spatially and temporally singlemode source, we can express the emitted two-mode squeezed

vacuum states as

$$|\Psi_{sq}\rangle = \sqrt{1-\lambda^2} \sum_{n=0}^{\infty} \lambda^n |n\rangle|n\rangle. \qquad (1)$$

where the photon number $|n\rangle = \frac{1}{\sqrt{n!}}\left(\hat{A}^\dagger\right)^n|0\rangle$ in a specific TM defined by the creation operator $\hat{A}^\dagger = \int d\omega f(\omega)\hat{a}^\dagger(\omega)$ and the generalized squeezing parameter $\lambda = \tanh(B)$. To experimentally realize such states, phasematching conditions and pump pulse properties need to support a factorable Joint Spectral Amplitude function. It has been shown that such conditions can be achieved via dispersion engineering [30], for example in non-linear waveguides.

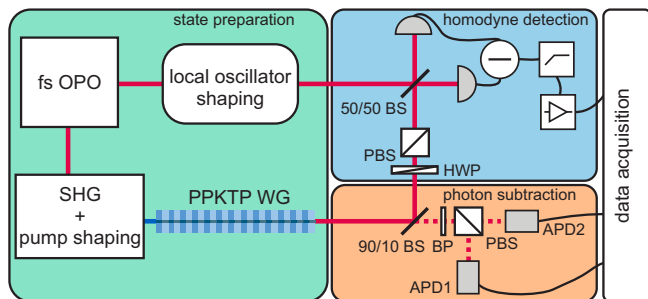Our experimental setup is described in figure 1, a mode-

FIG. 1. Schematic drawing of the experimental setup: the master OPO driving the experiment is frequency doubled to pump the PDC process while the remainder is spectrally shaped to serve as the LO for the HD detection. We interfere the signal and idler mode using a combination of half-wave plate (HWP) and a polarizing beam splitter (PBS), creating a single-mode squeezed beam which is then detected via a homodyne receiver.

locked fs laser, at a repetition rate of 82 MHz, is pumping a synchronously pumped optical parametric oscillator, central frequency at 1540 nm, wich is used to drive our experiment. It is frequency doubled via a periodically poled lithium niobate crystal, generating the pump for the SPDC process. The up-converted beam is then filtered via a 4f-spectrometer in order to ascertain the spectral decorrelation of the squeezed states via an optimized pump spectral width [30, 31]. We generate these states in a periodically poled potassium titanyl phosphate (PP-KTP) engineered waveguide chip under a type-II phase-matching. In order to achieve single TM emission, we choose the pump bandwidth to be 2.3 nm and its central wavelength to 769.6 nm so that we achieve the generation of frequency degenerate signal and idler beams around 1540 nm.

After the waveguide, we compensate for the birefringence of PPKTP so that signal and idler pulses temporarily overlap again. We realize the photon subtraction by tapping off a small portion of the two mode squeezed beams via a 90/10 beam splitter and filtered by a bandpass with 10 nm FWHM to suppress any background modes.

Thereafter, the modes are split using a polarizing beam splitter and subsequently sent onto an avalanche photodiode (APD) each. Coincidence signals from the APDs will then be forwarded to herald a successful photon subtraction in the signal and idler modes. Following the brighter port of the asymmetric beam splitter, signal and idler modes are interfered with each other on the combination of a half-wave plate and another polarizing beam splitter to generate a pair of single mode squeezed beams of which one is sent onto a homodyne receiver in order to record the quadrature data. The mixing of both modes of a two mode squeezed state here is the inversion of generating two mode squeezing by interfering two single mode squeezed beam on a symmetric beam splitter [32].

We characterize the properties by a number of DV measurement techniques using the APDs. A Hong-Ou-Mandel interference measurement gives us a visibility of 0.75 when interfering the signal and idler beams. The mean photon number $\langle n \rangle$ is estimated to be 0.56 photons per pulse which is equivalent to a two-mode squeezing of 6 dB. Finally, we estimate the number of effective time-frequency modes of our squeezed via a marginal $g^{(2)}$ measurement . It results in a value of $g^{(2)} = 1.81 \pm 0.05$ and thus to an effective mode number of 1.23 [33].

By seeding the PDC process with a coherent beam at 1540 nm and measuring the optical power at the detection stage, we estimate the efficiency of the optical elements of the squeezing path to be 0.87. The optimization of the homodyne receiver, mainly the modal overlap between the LO and the squeezed state, is achieved by using the visibility between the seeded PDC and an attenuated LO as figure of merit. We optimize the visibility by shaping the spectral amplitude and phase of the LO beam utilizing a commercially available waveshaper (Finisar waveshaper 4000s) and achieve a visibility of up to 0.91 between the seeded PDC and the LO field resulting in a receiver efficiency of about 0.72, when taking the quantum efficiency of 0.90 of the home-built homodyne detector into account.
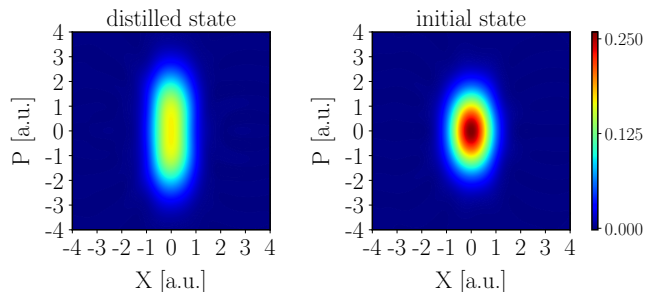
After having characterized the setup via DV meth-

FIG. 2. Contour plots of the reconstructed Wigner functions of the initial (right) and the distilled state (left) which is strongly deformed along the P quadrature.

ods, we measure the marginals of the Wigner function

sampled under a random angle due to the freely drifting phase between signal and the LO. For this, we record 250000 oscilloscope traces with a span of 100 μs and a sampling rate of $10^9 \frac{\text{Samples}}{s}$ each containing a single photon subtraction event surrounded by about 8000 squeezed states not subject to the photon subtraction. We assume, that the relative phase between squeezed light and LO stays constant during this time interval. This allows us to reconstruct the relative phase for every trace by using the variance of the squeezed states as a reference and, furthermore, allows us to directly compare the improvement in the quadrature variance due to the squeezing distillation.

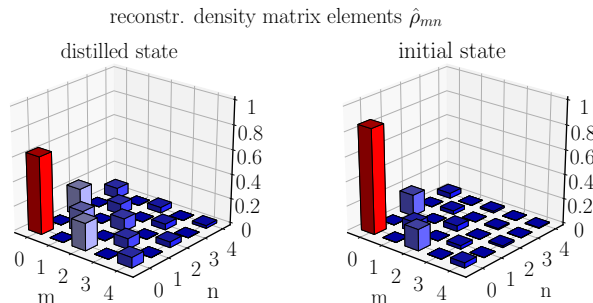Using the sorted homodyne data, we reconstruct the

FIG. 3. The first few elements of the reconstructed density matrices underlying the Wigner functions in Fig.2, for the distilled the higher order photon components become more pronounced as expected for this state.

density matrices for the distilled states and the squeezed reference states by means of a maximum likelihood reconstruction algorithm [34]. The results can be seen in figure 3. After successfully subtracting photons from both modes, the even higher order photon number component becomes more dominant for the distilled states which is equivalent to an increase in the squeezing. This can also be visualised when plotting the Wigner functions in fig. 2. While the undistilled initial state shows the expected elliptic shape of a regular squeezed state, the distilled state strongly deviates from this with an improvement in the squeezing quadrature and an even larger elongation of the Wigner function along the anti-squeezing quadrature. These results are summed up in table I and compared with a multi-mode theoretical model of the experiment. The initial state has a quadrature variance of -1.62 ± 0.01 dB relative to the shot noise as is expected when applying the overall system losses to the inferred squeezing of -6 dB. Due to the distillation step, this variance is improved to -1.72 ± 0.12 dB below shot-noise. This value have been calculated from the sorted raw data. Therefore, the statistics for the distilled events is limited thus increasing the standard deviation when compared to the undistilled squeezed state for which a greater number of states have been sampled. The anti-

squeezing in the orthogonal quadrature however experiences a noticeable increase from the initial 3.45 ± 0.01 dB to 6.21 ± 0.11 dB above shot-noise after the distillation procedure. This strong increase in anti-squeezing is expected and fits our theoretical model (see supplementary material).

In table I, we compare the reconstructed density matri-

TABLE I. Comparison of the quadrature variances and the purity of the reconstructed density matrices between the measured data and the results of multi-mode simulations

	$\hat{\rho}_{sq}$	$\hat{\rho}_{sq,sim}$	$\hat{\rho}_{dist}$	$\hat{\rho}_{dist,sim}$
$\text{Var}(\hat{X})[dB]$	-1.62 ± 0.01	-1.67	-1.72 ± 0.12	-1.89
$\text{Var}(\hat{P})[dB]$	3.45 ± 0.01	3.38	6.21 ± 0.11	6.06
$\text{tr}(\hat{\rho}^2)$	0.80	0.82	0.58	0.61

ces of the initial state $\hat{\rho}_{sq}$ and the distilled state $\hat{\rho}_{dist}$ with the simulation results $\hat{\rho}_{sq,sim}$ and $\hat{\rho}_{dist,sim}$ from the multi-mode model assuming the generation of a pure squeezed state (see supplementary material). The figure of merit in this case is the fidelity between density matrices of the squeezed and, respectively, the distilled states summed up in eq. 2.

$$\mathcal{F}_{dist} = 99.8\%, \qquad \mathcal{F}_{sq} = 99.9\% \qquad (2)$$

In Fig. 4, we illustrate the first four cumulants $\kappa_n, n \in \{1, 2, 3, 4\}$ of the Wigner function's marginal distribution as functions of the quadrature phase, where the projected quadrature is $\hat{X}_\theta = \cos\theta \ \hat{X} + \sin\theta \ \hat{P}$. In terms of the central moments $\mu_n = \left\langle \left(\hat{X}_\theta - \langle\hat{X}_\theta\rangle \right)^n \right\rangle$ and the mean value m_1, the cumulants can be expressed in a compact form as

$$\kappa_1 = m_1, \qquad \kappa_2 = \mu_2$$
$$\kappa_3 = \mu_3, \qquad \kappa_4 = \mu_4 - 3\mu_2^2 \qquad (3)$$

Gaussian distributions, such as the Wigner functions of pure squeezed states are fully determined by the first and second cumulant, i.e. by the mean value and the variance. Hence, particularly the higher order cumulants characterize the peculiarities of the distilled state [35]. The third and fourth cumulant are associated with the skewness and the 'tailedness' (kurtosis) of the distributions. For the undistilled state, we find that, apart from statistical fluctuations, only the variance $\kappa_2(\theta) = \text{Var}(X_\theta)$ is non-zero and shows the expected transition from squeezing $\text{Var}(X_\theta) < 1$ to anti-squeezing $\text{Var}(X_\theta) > 1$. For the distilled state, we find a similar behaviour for $\kappa_2(\theta)$, however, with larger squeezing and anti-squeezing values. Moreover, we find that the kurtosis $\kappa_4(\theta)$ is non-zero and shows a clear trend to negative values when rotating the projected quadrature from the squeezing to the anti-squeezing angle. A negative kurtosis is a non-Gaussian feature showing that the distribution is flatter than a normal distribution. This fits
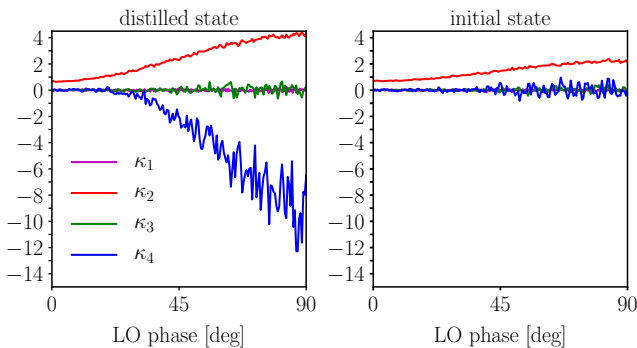
FIG. 4. Cumulants calculated from the raw data of the initial (right) and the distilled squeezed state (left) for different LO phases binned in steps of 0.5 degrees: for the initial state, all cumulants except for the variance are centered around 0, as expected for a Gaussian state. The distilled state however shows a negative kurtosis with increasing phase, strongly hinting at its non-Gaussian nature.

well with the observed elongation of the Wigner function along the P quadrature in figure 2 which is follows the prediction of our theoretical model.

In conclusion, we have shown that source engineering offers a practical solution to overcome the difficulties when realizing hybrid quantum information protocols. This we showcase by using our engineered PDC source of pulsed squeezed states with high purity and amounts of detected squeezing. We achieved these results using source engineering, which we have shown to be a viable alternative to conventional approaches using spectral and spatial filtering. We further demonstrated a possible application of our source in hybrid quantum information processing by realizing a squeezing distillation experiment using this source. We detected an improvement in the measured squeezing and confirmed the expected non-Gaussian quadrature statistics using the higher order statistical cumulants. All-together, these results highlight the applicability of source engineering in a hybrid quantum information processing context as well as the suitability of our source to be a building block for the realization of larger hybrid quantum networks and quantum computers.

[1] H. Vahlbruch, M. Mehmet, K. Danzmann, and R. Schnabel, Phys. Rev. Lett. **117**, 110801 (2016).
[2] M. Förtsch, G. Schunk, J. U. Fürst, D. Strekalov, T. Gerrits, M. J. Stevens, F. Sedlmeir, H. G. L. Schwefel, S. W. Nam, G. Leuchs, and C. Marquardt, Phys. Rev. A **91**, 023812 (2015).
[3] N. Takanashi, W. Inokuchi, T. Serikawa, and A. Furusawa, Opt. Express **27**, 18900 (2019).
[4] A. Eckstein, A. Christ, P. J. Mosley, and C. Silberhorn, Phys. Rev. Lett. **106**, 013603 (2011).
[5] G. Harder, V. Ansari, B. Brecht, T. Dirmeier, C. Marquardt, and C. Silberhorn, Opt. Express **21**, 13975 (2013).
[6] K.-i. Yoshino, T. Aoki, and A. Furusawa, Applied Physics Letters **90**, 041111 (2007).
[7] Y.-S. Ra, C. Jacquard, A. Dufour, C. Fabre, and N. Treps, Physical Review X **7**, 031012 (2017).
[8] V. Ansari, G. Harder, M. Allgaier, B. Brecht, and C. Silberhorn, Physical Review A **96**, 063817 (2017).
[9] G. Harder, T. J. Bartley, A. E. Lita, S. W. Nam, T. Gerrits, and C. Silberhorn, Phys. Rev. Lett. **116**, 143601 (2016).
[10] R. J. A. Francis-Jones, R. A. Hoggarth, and P. J. Mosley, Optica **3**, 1270 (2016).
[11] N. Bruno, A. Martin, T. Guerreiro, B. Sanguinetti, and R. T. Thew, Opt. Express **22**, 17246 (2014).
[12] F. Kaneda, K. Garay-Palmett, A. B. U'Ren, and P. G. Kwiat, Opt. Express **24**, 10733 (2016).
[13] A. Christ, C. Lupo, M. Reichelt, T. Meier, and C. Silberhorn, Phys. Rev. A **90**, 023823 (2014).
[14] J. Eisert, S. Scheel, and M. Plenio, Phys. Rev. Lett. **89**, 137903 (2002).
[15] E. Knill, R. Laflamme, and G. J. Milburn, Nature **409**, 46 (2001), article.
[16] S. Lloyd and S. L. Braunstein, Phys. Rev. Lett. **82**, 1784 (1999).
[17] U. L. Andersen, J. S. Neergaard-Nielsen, P. Van Loock, and A. Furusawa, Nature Physics **11**, 713 (2015).
[18] J. Heersink, C. Marquardt, R. Dong, R. Filip, S. Lorenz, G. Leuchs, and U. L. Andersen, Phys. Rev. Lett. **96**, 253601 (2006).
[19] R. Dong, M. Lassen, J. Heersink, C. Marquardt, R. Filip, G. Leuchs, and U. L. Andersen, Nature Physics **4** (2008).
[20] B. Hage, A. Samblowski, J. DiGuglielmo, A. Franzen, J. Fiurásek, and R. Schnabel, Nature Physics **4** (2008).
[21] A. E. Ulanov, I. A. Fedorov, A. A. Pushkina, Y. V. Kurochkin, T. C. Ralph, and A. I. Lvovsky, Nature Photonics **9**, 764 EP (2015), article.
[22] O. Morin, K. Huang, J. Liu, H. Le Jeannic, C. Fabre, and J. Laurat, Nature Photonics **8**, 570 (2014).
[23] H. Jeong, A. Zavatta, M. Kang, S.-W. Lee, L. S. Costanzo, S. Grandi, T. C. Ralph, and M. Bellini, Nature Photonics **8**, 564 (2014).
[24] G. Masada, K. Miyata, A. Politi, T. Hashimoto, J. L. O'brien, and A. Furusawa, Nature Photonics **9**, 316 (2015).
[25] A. E. Ulanov, D. Sychev, A. A. Pushkina, I. A. Fedorov, and A. Lvovsky, Phys. Rev. Lett. **118**, 160501 (2017).
[26] E. Agudelo, J. Sperling, L. Costanzo, M. Bellini, A. Zavatta, and W. Vogel, Phys. Rev. Lett. **119**, 120403 (2017).
[27] J. Wenger, R. Tualle-Brouri, and P. Grangier, Phys. Rev. Lett. **92**, 153601 (2004).
[28] Y. Kurochkin, A. S. Prasad, and A. Lvovsky, Phys. Rev. Lett. **112**, 070402 (2014).
[29] H. Takahashi, J. S. Neergaard-Nielsen, M. Takeuchi, M. Takeoka, K. Hayasaka, A. Furusawa, and M. Sasaki, Nature photonics **4**, 178 (2010).

[30] A. B. U'Ren, C. Silberhorn, K. Banaszek, R. E. Ian A. Walmsley, W. P. Grice, and M. G. Raymer, Laser-Physics **15** (2005).

[31] W. P. Grice, A. B. U'Ren, and I. A. Walmsley, Phys. Rev. A **64**, 063815 (2001).

[32] C. Silberhorn, P. K. Lam, O. Weiß, F. König, N. Korolkova, and G. Leuchs, Phys. Rev. Lett. **86**, 4267 (2001).

[33] A. Christ, K. Laiho, A. Eckstein, K. N. Cassemiro, and C. Silberhorn, New Journal of Physics **13**, 033027 (2011).

[34] J. Řeháček, Z. c. v. Hradil, E. Knill, and A. I. Lvovsky, Phys. Rev. A **75**, 042108 (2007).

[35] C. R. Müller, G. Leuchs, C. Marquardt, and U. L. Andersen, Phys. Rev. A **96**, 042311 (2017).

[36] T. J. Bartley and I. A. Walmsley, New Journal of Physics **17**, 023038 (2015).

SUPPLEMENTARY MATERIAL: DISTILLATION OF SQUEEZING USING AN ENGINEERED PDC SOURCE

Here, we briefly describe, how we theoretically modelled our squeezing distillation protocol shown in the main paper and which assumptions are made to result at the theoretically expected values. We start with the usual two mode squeezed vacuum state which is often generated using a SPDC process in a non-linear material

$$|\psi\rangle = \sqrt{1-\lambda^2} \sum_n \lambda^n |n,n\rangle \qquad (1)$$

with squeezing strength $\lambda = \tanh(B)$ given by the parametric gain B. The generation process is usually described in the Heisenberg picture as

$$|\Psi\rangle = \exp[-\frac{i}{\hbar}B \int d\omega_s d\omega_i f(\omega_s,\omega_i)$$
$$\times \hat{a}_s^\dagger(\omega_s)\hat{b}_i^\dagger(\omega_i) + h.c.]|0\rangle. \qquad (2)$$

Here, the joint spectral amplitude (JSA) function $f(\omega_s,\omega_i) = \alpha(\omega_s,\omega_i)\Phi(\omega_s,\omega_i)$, which is the product from phasematching function and the pump field envelope, describes the range of allowed signal and idler frequencies in the PDC process at hand. In general however, the JSA can be decomposed in a set of mutually orthogonal modes using the Schmidt decomposition $f(\omega_s,\omega_i) = \sum_k c_k g_k(\omega_s)h_k(\omega_i)$ with Schmidt coefficients following the normalisation condition $\sum_k c_k^2 = 1$ [5, 33]. As such, the state generated in a PDC process can be rewritten in terms of the Schmidt decomposition which results in general in a mixed state of a multitude of individually two-mode squeezed beams

$$|\Psi\rangle = \exp[-\frac{i}{\hbar}B \int d\omega_s d\omega_i \sum_k c_k \hat{A}_{k,s}^\dagger \hat{A}_{k,i}^\dagger + h.c.]|0\rangle$$
$$= \bigotimes_k |\psi^{(k)}\rangle. \qquad (3)$$

with the broadband mode creation operators $\hat{A}_k = \int d\omega\, \hat{a}(\omega)f_k(\omega)$ and their mode dependent squeezing strength $\lambda_k = \tanh(c_k\, B)$.

To account for this multimode nature of the produced PDC state is essential for the performance of our distillation protocol. In fig. 1, we show a graphic representation of our protocol. After the generation of the signal and idler beams, we independently split of a small part and send it towards a pair of avalanche photodiodes (APD). The remaining beams are interfered and finally, the quadrature data of one of the output port of the interference beamsplitter is recorded using homodyne detection which is triggered by a successful registration of a coincidence of the APDs. It is important to note, that neither the beamsplitters nor the APDs exhibit any mode-selective characteristic. Therefore, it is possible that the APDs register coincidence events stemming from photons in a mode orthogonal to the LO mode or a combination of the LO mode and one other Schmidt mode which in turn lead to a "false" trigger event which
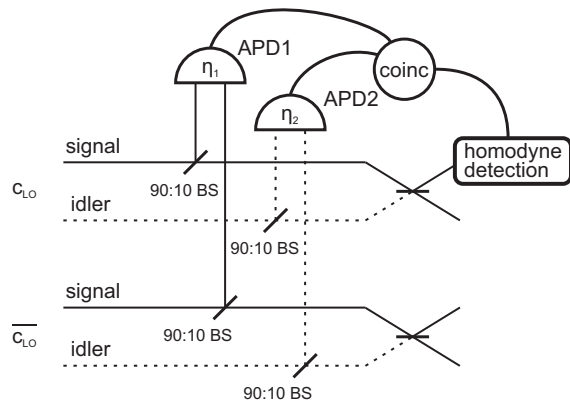

FIG. 1. Schematic picture of the distillation scheme used in the paper. Signal and idler Photons are subtracted from a randomly determined spectral mode after passing an asymmetric beamsplitter with T = 0.9 and belong either to the mode selected by the LO c_{LO} or any of the other, orthogonal, modes $\bar{c}_{LO}$. On the registration of a coincidence event between the two APDs, the homodyne data is taken and stored.

results in detecting an ordinary squeezed state with the homodyne receiver or a state with only one photon subtracted in either the signal or idler mode.

To appropriately model the experimental situation, the measured state has to be in the form

$$\hat{\rho} = \alpha_0\hat{\rho}_{sub(2)} + \alpha_1\hat{\rho}_{sub(1)} + \alpha_2\hat{\rho}_{sq} \qquad (4)$$

the coefficients α_i denote the relative frequencies of the two photon subtracted state $\hat{\rho}_{sub(2)}$, the one photon subtracted state $\hat{\rho}_{sub(1)}$, or the "ordinary" squeezed state $\hat{\rho}_{sq}$ and fulfil the condition $\sum \alpha_i = 1$. The density matrices describing the separate measurement outcomes are calculated using analytic formulas given in [36].

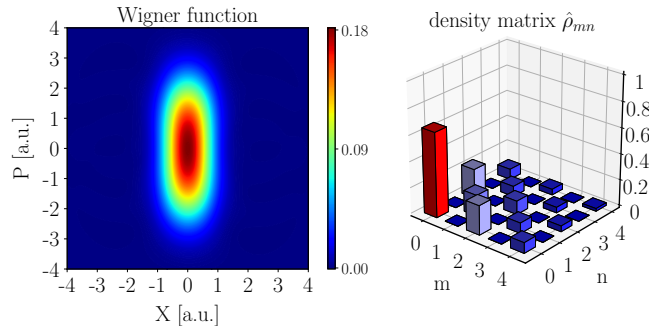In order to calculate the coefficients α_i, we start calcu-

FIG. 2. Wigner function of the simulated state, given by eq. 4, for the parameters given by our experimental findings in the main paper. Both show a good qualitative agreement with the results of the state reconstruction performed on the experimental data.

lating the detection probabilities of coincidences in the

heralding arms starting from the initial state:

$$p_{mn}^{(k)} = tr\left(|m,n\rangle\langle m,n|_k \hat{\rho}_{sq}^{(k)}\right) \tag{5}$$

The detection probabilities in the APD arms can then be obtained via the binomial distributions $L_{i,j} = \sum_j \binom{j}{i}\eta^i(1-\eta)^{j-i}$ modelling the random linear loss due to optical and detection loss described by η.

$$p_{m'n'}^{\prime(k)} = \sum_{m,n} L_{m'm}\, p_{mn}^{(k)}\, L_{n'n} \tag{6}$$

The indices $\{m,n\}$ here represent the signal and idler modes individually, while k denotes the order of the different spectral modes. To each of the subtraction detectors, a detection probability η_i with $i \in \{1,2\}$ can be assigned to. In general, these probabilities are of different magnitude, in our simulations however, we assume both of them to be identical.

Whereas, we calculate the different probabilities under the assumption that only the first two Schmidt modes are relevant due to the high value of $g^{(2)}$ and further that the any photon number contributions of order higher than two can be be neglected due to the overall heralding efficiency $\eta \approx 0.02$. We define shorthand expressions for the probabilities of the different detection events as:

$$\begin{aligned}
p_{1100}' &= p_{11}^{\prime(0)} p_{00}^{\prime(1)} \\
p_{0011}' &= p_{00}^{\prime(0)} p_{11}^{\prime(1)} \\
p_{1001}' &= p_{0110}' = p_{10}^{\prime(0)} p_{01}^{\prime(1)}
\end{aligned} \tag{7}$$

Using the normalization condition of the coefficients α_i, we model the ratio between the number of coincidences stemming from the desired distillation events and the unwanted events to be given by the ratio of the respective probabilities

$$\frac{\alpha_0}{\alpha_1 + \alpha_2} \approx \frac{p_{1100}'}{2p_{1001}' + p_{0011}'} \tag{8}$$

The coefficients α_i themselves are then given by the following expressions

$$\begin{aligned}
\alpha_0 &= \frac{p_{1100}'}{p_{1100}' + p_{0011}' + 2p_{1001}'} \\
\alpha_1 &= \frac{2p_{1001}'}{p_{1100}' + p_{0011}' + 2p_{1001}'} \\
\alpha_2 &= \frac{p_{0011}'}{p_{1100}' + p_{0011}' + 2p_{1001}'}
\end{aligned} \tag{9}$$

allowing us to construct the density matrix of the final state. From there, we calculate the density matrix given in eq. 4 and the Wigner function of the mixed final state for our model, both shown in figure 2. The simulation results show a good qualitative agreement with the experimental findings in the main paper with a squeezing value of -1.89dB with an accompanying anti-squeezing value of 6.06dB relative to shot noise. The lower anti-squeezing value can be attributed to the assumption of the generation of a pure state in PDC crystal and the neglection of any processes introducing excess noise.